HAL
open science

Reversibility Of Superconducting Nb Weak Links Driven By The Proximity Effect In A Quantum Interference Device

Nikhil Kumar, Thierry Fournier, Hervé Courtois, Clemens Winkelmann, Anjan K. Gupta

To cite this version:

Nikhil Kumar, Thierry Fournier, Hervé Courtois, Clemens Winkelmann, Anjan K. Gupta. Reversibility Of Superconducting Nb Weak Links Driven By The Proximity Effect In A Quantum Interference Device. Physical Review Letters, 2015, 114 (15), pp.157003. 10.1103/PhysRevLett.114.157003 . hal-01158766

HAL Id: hal-01158766

https://hal.science/hal-01158766

Submitted on 5 Jun 2015

HAL is a multi-disciplinary open access archive for the deposit and dissemination of scientific research documents, whether they are published or not. The documents may come from teaching and research institutions in France or abroad, or from public or private research centers.

L'archive ouverte pluridisciplinaire **HAL**, est destinée au dépôt et à la diffusion de documents scientifiques de niveau recherche, publiés ou non, émanant des établissements d'enseignement et de recherche français ou étrangers, des laboratoires publics ou privés.

arXiv:1411.7196v2 [cond-mat.supr-con] 4 Jun 2015

Reversibility of Superconducting Nb Weak Links Driven by the Proximity Effect in a Quantum Interference Device

Nikhil Kumar,[1] T. Fournier,[2,3] H. Courtois,[2,3] C. B. Winkelmann,[2,3] and Anjan K. Gupta[1]

[1] *Department of Physics, Indian Institute of Technology Kanpur, Kanpur 208016, India*
[2] *Université Grenoble Alpes, Institut Néel, F-38042 Grenoble, France*
[3] *CNRS, Institut Néel, F-38042 Grenoble, France*

(Dated: June 5, 2015)

We demonstrate the role of proximity effect in the thermal hysteresis of superconducting constrictions. From the analysis of successive thermal instabilities in the transport characteristics of micron-size superconducting quantum interference devices with a well-controlled geometry, we obtain a complete picture of the different thermal regimes. These determine whether the junctions are hysteretic or not. Below the superconductor critical temperature, the critical current switches from a classical weak-link behavior to one driven by the proximity effect. The associated small amplitude of the critical current makes it robust with respect to the heat generation by phase-slips, leading to a non-hysteretic behavior.

Micron-size superconducting quantum interference devices (μ-SQUID), based on superconducting (SC) weak links (WLs), have been of interest for probing magnetism at small scales [1–8]. A major obstacle of a μ-SQUID proper operation is its hysteretic current-voltage characteristic (IVC). During current ramp-up, the WL switches to a dissipative state at the critical current I_c and during current ramp-down, it comes back to a zero-voltage state at the re-trapping current $I_r < I_c$. In conventional tunnel-barrier type Josephson-junctions, the hysteresis arises from large junction capacitance [9]. In WLs with negligible capacitance, hysteresis is found at low temperatures below a crossover temperature $T_h < T_c$ [10], with T_c as the SC critical temperature. Although an effective capacitance can arise from the recovery time of the SC order parameter [11], it is now understood that hysteresis in WLs is of thermal origin [14–16], similar to that observed in SNS WLs [12]. A Recent report on high-T_c-SC based μ-SQUID shows non-hysteretic IVCs over a wide temperature range [13]. Thermal hysteresis in WLs and its effect on IVCs has been modeled by local thermal balance dictating the position of normal metal-superconductor (N-S) interface [14–16]. In case of poor heat evacuation, phase fluctuations can trigger a thermal run-away giving a resistive hot-spot. This topic is of great practical importance, in particular for SC-magnet wires and cables, helium level sensors, bolometers [17], μ-SQUIDs and other nano-scale SC structures [18]. A systematic understanding of various thermal phases which a WL device exhibits can help designing non-hysteretic devices.

In this Letter, we report on the transport characteristics of Nb-film based μ-SQUIDs with a well-controlled geometry and describe a complete picture of different thermal regimes. The IVCs show a critical current and two re-trapping currents that we describe using a thermal instability model in SC leads. The critical current I_c follows the theoretical expectation at low temperature but changes its behavior while crossing the smaller re-trapping current. In this hysteresis-free regime, the WLs superconduct, despite being slightly heated by individual phase slips, thanks to the proximity effect of the adjacent SC.

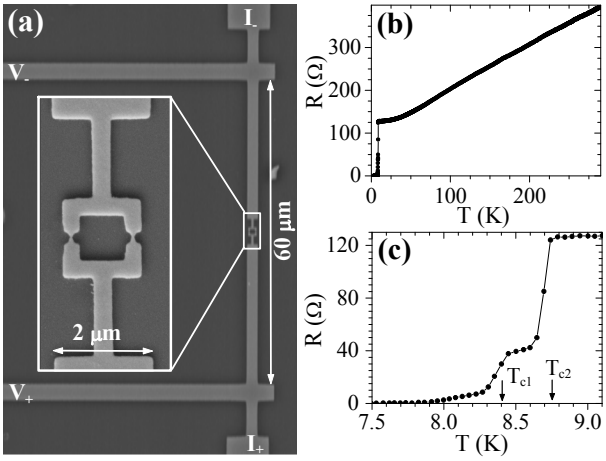

FIG. 1: (a) SEM image of the μ-SQUID μS1 with its current and voltage leads. The zoomed-in image shows the SQUID loop (with area 1×1 μm^2) and the narrow leads. (b) Resistance vs temperature (R-T) plot. (c) Low-temperature portion of the R-T plot for μS1 at 0.01 mA current.

We fabricated [22] μ-SQUIDs from Nb films using common techniques [2, 19, 20]. The transport measurements were carried out down to 4.2 K temperature in a home-made cryostat with built-in copper-powder filters [10]. We have studied six devices with similar behavior, but here we report on two devices, μS1 and μS2. For all devices, the patterned SQUID-loop area is 1 μm^2 and the width of its arms is 0.3 μm. The designed WL length is 150 nm while the WL width is 70 and 50 nm in μS1 and μS2, respectively. Fig. 1(a) shows the SEM image of μS1. Four different parts of the pattern contribute to the electrical characteristics, namely, 1) the two WLs, each of normal resistance R_{WL}, 2) the SQUID loop with normal

resistance as R_L including the WLs, 3) the narrow leads of width 0.3 μm and length 1.7 μm on either side of the SQUID loop, each with a resistance R_1, and 4) the wide leads of width 2 μm, length 27.5 μm and normal resistance R_2. From the geometry, the total normal-state resistance between the voltage leads is $R_N = R_L + 2R_1 + 2R_2 = 40.3R_\square + 0.5R_{WL}$. Here, $R_\square$ is the film's square resistance.

Figure 1(b) and (c) show the resistance R Vs temperature for μS1. Multiple SC transitions are observed. The resistance jumps from its residual value of 128 Ω down to about 40 Ω at $T_{c2} = 8.7$ K, jumps further down from 38 to 8 Ω at $T_{c1} = 8.35$ K, and finally decreases smoothly to zero. We attribute the transition at T_{c2} to the wide leads and that at T_{c1} to both the narrow leads and the SQUID loop. From IVC in non-hysteretic regime, discussed later [see Fig. 3(f)], we deduce $R_{WL} \simeq 8$ Ω. This analysis is consistent with $R_\square = 3.1$ Ω, giving a resistivity of 9.5 $\mu\Omega$.cm.

Next we discuss a one-dimensional model of thermal instability in long current-biased SC leads. This is similar to Broom and Rhoderick [21] model on the dynamics of an N-S interface under the influence of a current. Thus a critical magnitude of current is found at which the N-S interface changes its direction of motion. Here we consider a SC lead with normal state resistivity ρ_n, uniform thickness t and width w, and carrying an electrical current I as shown in Fig. 2(a). The heat transfer with the substrate at a bath temperature T_b writes $\alpha(T - T_b)/t$, where α is a characteristic of the interface. The thermal conductivity κ is constant and uniform. An N-S interface exists at $x = 0$, so at this point $T = T_c$. A heat current flows from $x < 0$ due to the resistance of this lead portion plus possibly a device at the end of the lead. With the boundary condition $T = T_b$ at $x \to \infty$, the heat equation solution for $x > 0$ is $T = T_b + (T_c - T_b)\exp(-x/l_{th})$. The thermal healing length $l_{th} (= \sqrt{\kappa t/\alpha})$ is a crossover length-scale such that for $\Delta x \gg l_{th}$ substrate heat-loss dominates and for $\Delta x \ll l_{th}$ conduction dominates. The heat current at the N-S interface ($x = 0$) is then $\dot{Q}_0 = w\alpha l_{th}(T_c - T_b)$ implying an effective thermal resistance of $(w\alpha l_{th})^{-1}$ as seen from the N-S interface. It is important to realize that the N-S interface will shift to the right (left) if more (less) than $\dot{Q}_0$ heat is incident on the lead at $x = 0$.

For analyzing the stability of the N-S interface, we look into the effect of fluctuations on a differential element (from $x = 0$ to $x = dx$) at this interface in a quasi-static approximation. If this element turns resistive, see Fig. 2(b), an additional power $I^2\rho_n dx/(wt)$ is generated, which is shared equally between the left and right interfaces to the lead and the substrate receives a negligible amount [22]. The heat current across the new N-S interface is $\dot{Q}'_1 = \dot{Q}_0 - \alpha(T_c - T_b)wdx + I^2\rho_n dx/(2wt)$. As pointed out before, if this heat is more (less) than $\dot{Q}_0$, the N-S interface will shift to the right (left) implying instability (stability). Thus the maximum current that

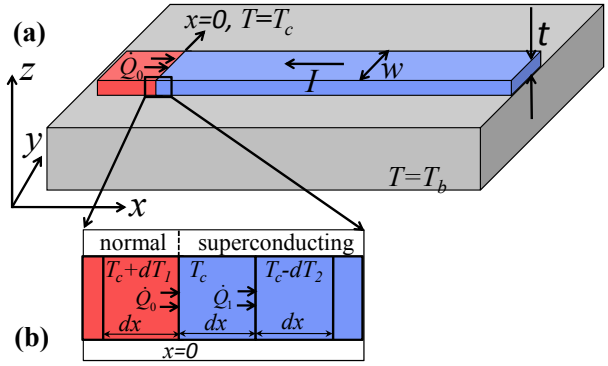

FIG. 2: (a) Schematic of the semi-infinite (in $+x$ direction) lead of SC material on a substrate at T_b with N-S interface at $x = 0$. (b) shows the region near the N-S interface with three differential elements of length dx when the N-S interface stabilizes near the heat source on left.

the lead can carry without causing a thermal instability is given by,

$$I_{max} = w\sqrt{2\alpha(T_c - T_b)/R_\square}. \quad (1)$$

This expression is consistent with Ref. [14] results in long lead limit and equal thermal conductivities of SC and normal metal, which is valid close to the N-S interface. When I exceeds I_{max}, the N-S interface will runaway to a large x location where the lead joins a thermal bath (or a much wider lead). By analyzing the stability of a small resistive element against an incursion to the SC state, one finds as expected the same expression for the re-trapping current. It would be more appropriate to call I_{max} as the 'instability current' as it describes both the runaway and re-trapping of the N-S interface. We will use the term 're-trapping' current, as it has been done in most earlier works.

In order to quantify the relevant parameters, we use the Wiedemann-Franz law, i.e. $\kappa = LT/\rho$ with $L = 2.44\times10^{-8}$ W.Ω/K^2 as the Lorenz number, and using $T = T_c = 8.5$ K and $\rho = 9.5$ $\mu\Omega$.cm, we get $\kappa = 2.4$ W/m.K. Typical values of α used in literature [14, 16] range from 1 to 10 W/cm^2.K. We use $\alpha = 5.3$ W/cm^2.K as found from the temperature dependence of a re-trapping current as discussed later. Thus we find $l_{th} = 1.6$ μm for our devices, which is much smaller than the length of the wide leads and comparable to that of the narrow leads.

IVCs of μS1 in Fig. 3 shows sharp jumps in voltage at three currents, namely I_{r1}, I_{r2} and I_c. The jump at I_c occurs during the current ramp up from zero with a distribution in its value. Thus for μS1 I_c has a width [22] of about 40 μA with a mean value of 1.3 mA at 4.2 K, in agreement with the expected de-pairing current [23]. From the IVC slope, the resistance just above I_{r1} is about 48 Ω. This value is close to the sum $R_L + 2R_1 = 40$ Ω,

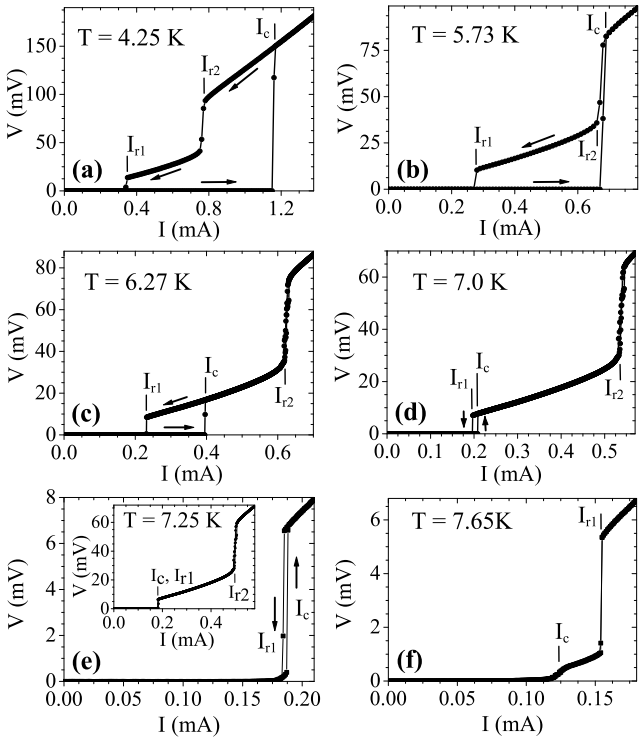

FIG. 3: (a) - (d) IVCs in hysteretic regime for μS1 at different temperatures. A large hysteresis is seen at 4.25 K with two re-trapping currents, I_{r1} and I_{r2}. I_c crosses I_{r2} near 5.7 K and I_{r1} around 7.25 K as seen in (e). (f) shows the IVC of μS1 in the non-hysteretic regime above T_h = 7.25 K. The inset of (e) shows a larger bias-current range plot to show the I_{r2} transition.

which means that the SQUID loop and the narrow leads are heated to above T_c for $I > I_{r1}$. The observed higher value indicates that a portion of the wide leads is also heated to above its T_c. The IVC slope above the second re-trapping current I_{r2} is 140 Ω, which is close to the measured residual resistance value, i.e. 128 Ω, indicating a thermal runaway till the voltage leads. The slightly larger value seen here is due to the heating in the central portion to more than 50 K as estimated from a thermal model. At higher temperatures when I_{r2} is much less, indicating reduced heating, the slope above I_{r2} is found to be 128 Ω. In this regime, Fig. 3(f) shows that the resistance just above I_c is about 4 Ω giving R_{WL} = 8 Ω. Only the critical current I_c was found to oscillate with the magnetic flux [22] as expected for a SQUID. The retrapping currents $I_{r1,2}$ do not, implying a different origin than the SC of the WL.

The three currents I_{r1}, I_{r2} and I_c evolve differently with temperature. Near 5.7 K, I_c crosses I_{r2} [see Fig. 3(b)] and at $T = T_h$ = 7.25K, I_c crosses I_{r1} [see Fig. 3(e)], so the hysteresis is absent at higher temperatures [see Fig. 3(f)]. In non-hysteretic regime above T_h, the IVC near I_c becomes relatively smooth while the voltage jump at I_{r1} remains sharp and evolves over this smooth feature. Also, the hysteresis does not disappear till I_{r1} fully crosses this smooth feature [see Fig.3(e)].

Figure 4(a) summarizes the bath-temperature dependence of I_c, I_{r1} and I_{r2} for μS1. Fig. 4(b) shows the same for the device μS2, with a smaller critical current, and thus a smaller T_h. The retrapping currents $I_{r1,2}$ are the same in the two samples confirming that these are independent of the WL structure. With increasing T_b, I_c decreases linearly in both devices up to T_h, where it shows a marked change in behavior. For both devices, I_c and I_{r1} go to zero at T_{c1}, while I_{r2} vanishes at T_{c2}. This is consistent with the R-T behavior of Fig. 1(c). In both plots, we also indicate the state (resistive or SC) of different portions of the device when the current is ramped down, which constitutes a kind of a phase-diagram, or more appropriately, state-diagram. The light gray-shaded area shows the bistable region where the whole device is SC during the current ramp-up from zero. In the dark gray-shaded region, only the WLs are resistive. No hysteresis is observed in the related temperature range [T_h,T_{c1}]. This is the most desirable mode for a SQUID, but it occurs in quite a limited temperature window. At a fixed current bias, we do see the expected voltage oscillations with flux in this regime [22].

Using the long lead approximation for the wide leads, we can fit I_{r2} with Eq. 1 which writes here $I_{r2} = w\sqrt{2\alpha(T_{c2} - T_b)/R_\square}$. We obtain a very good fit, see Fig. 4 with the only free parameter being α = 5.3 W/cm^2.K, in good agreement with reported values [14, 16]. With the same parameters, except w = 0.3 μm, Eq. 1 predicts for the narrow leads a current I_{r1} significantly smaller than observed. This is expected as the presence of wide leads at a short distance makes the heat evacuation more efficient, leading to a higher run-away current.

In a WL with dimensions less than the SC coherence length, we expect, close to its T_c, $I_c R_{WL} = \beta(T_c - T_b)$ with β = 0.635 mV/K [3]. Our devices are in the Josephson regime [3], at least close to T_c. From the I_c slope in Fig. 4(a) for μS1 at temperatures below T_h, we find a $R_{WL}/2$ value of 3 Ω, which agrees with our earlier findings. In this same regime, the extrapolated T_c value of 7.4 K is related to the intrinsic SC of the WLs. Above T_h, the T_b dependence of I_c changes slope and I_c goes to zero precisely at T_{c1}. Hence we conclude that the WLs are SC above T_h owing to proximity effect from the adjacent SC with a higher T_c.

Finally, we elaborate on how the behavior change of I_c coincides with T_h. Below T_h, I_c exceeds the stability current I_{r1}. In this case, even a single phase-slip event induced by thermal fluctuations can cause a thermal runaway [18]. IVCs thus exhibit a sharp voltage jump at I_c with a distribution in I_c values [24] because the transition is caused by stochastic fluctuations. Above T_h, $I_c < I_{r1}$, so that no thermal runaway can happen at I_c: the reversible (mono-stable) regime is obtained. The

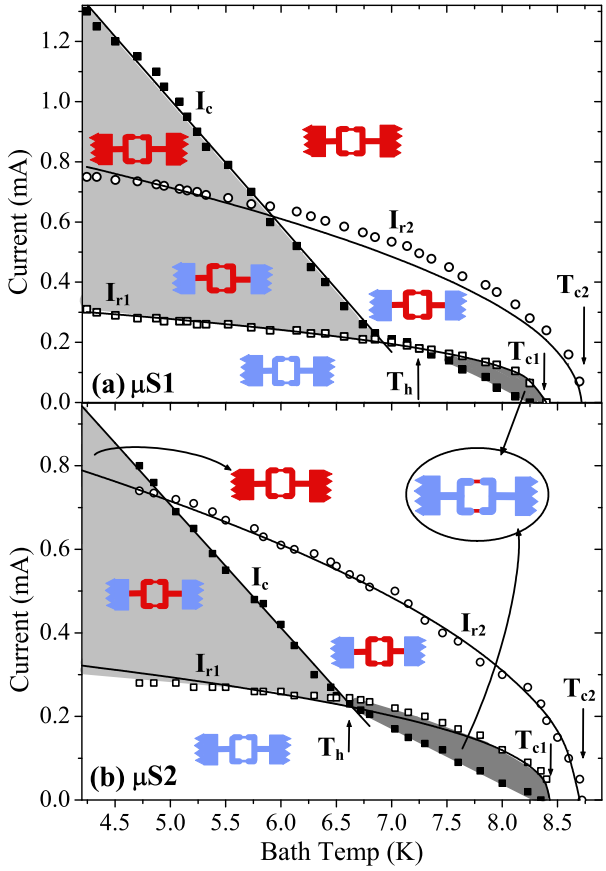

FIG. 4: Variation of I_c, I_{r1} and I_{r2} with T_b for **(a)** μS1 and **(b)** μS2. The symbols are the data points. The continuous lines are fits given by (in mA and K), **(a)** $I_c = 0.42(7.4 - T_b)$ and **(b)** $I_c = 0.29(7.4 - T_b)$ while the other two are described by $I_{r1} = 0.17(8.4 - T_b)^{0.43}$ and $I_{r2} = 0.37(8.7 - T_b)^{0.5}$ for both the devices. The cartoon pictures of the device shown in different regions depict the state of the device during current ramp-down with blue as SC and red as resistive portions. The light gray-shaded area shows the bistable region where the whole device is in the fully SC state during the current ramp-up from zero. In the dark gray-shaded region, only WLs are resistive.

transition to the resistive state (at I_c) is smeared with a finite voltage below I_c, see Fig. 3(e). This is due to phase-slip proliferation as the energy barrier for phase-slip is small for currents close to I_c [24]. The related dissipation just below I_c also heats some portion of the device above T_b. Assuming that the whole SQUID loop is at nearly uniform temperature, which is justified since its size is comparable to l_{th}, we estimate that the power generated just below I_c of 72 nW for $T_b = 7.25$ K brings the SQUID loop to a temperature of about 7.8 K. Because of this and of the fact that the WL region is actually a SC with a lower T_c, the T_b dependence of I_c between T_h and T_{c1} cannot be simply described by that of S-N-S WLs [25]. Nevertheless, close to T_c we can expect a linear temperature dependence as is the case with both SNS WL and constriction [3]. The heating will reduce I_c value and the exact temperature dependence, close to T_c, would be sub-linear.

I_c and I_{r1} are expected to cross at some temperature even if the WL T_c is same as that of the adjacent SC. But then the reversible regime will exist over a narrower temperature range. Thus the smaller T_c of the WL and the proximity SC plays crucial role in widening this hysteresis-free temperature range. By reducing the width of the constriction while keeping other dimensions same one can reduce I_c without affecting I_{r1}. This will definitely widen the temperature range of reversible operation. Although at extremely low temperatures, due to divergent Kapitza resistance making α approach zero, the hysteresis is expected to occur even for very small I_c. This regime is yet to be investigated.

In conclusion, we present the complete device-state diagram of Nb based μ-SQUIDS. We highlight a non-classical weak link behavior which is understood in the framework of a thermal instability picture. The non-hysteretic high temperature regime of the weak-links is shown to benefit from proximity superconductivity. The present new understanding of the physical mechanisms at the origin of a non-hysteretic behavior is key to further developments in μ-SQUID magneto-sensors for which the suppression of hysteresis represents a key issue.

Samples were fabricated at the platform Nanofab, CNRS Grenoble and measurements were carried out in IIT Kanpur. AKG thanks University Joseph Fourier for a visiting fellowship. NK acknowledges the financial support from CSIR, India. This work has been financed by the French Research National Agency, ANR-NanoQuartet (ANR12BS1000701) and the CSIR of the govt. of India.

[1] W. Wernsdorfer, Adv. Chem. Phys. **118**, 99 (2001).
[2] K. Hasselbach, C. Veauvy, D. Mailly, Physica C **332**, 140 (2000).
[3] K. K. Likharev, Rev. Mod. Phys. **51**, 101 (1979).
[4] D. Hazra, J. R. Kirtley, and K. Hasselbach, Appl. Phys. Lett. **103**, 093109 (2013).
[5] D. Vasyukov, et. al., Nature Nanotech. **8**, 639 (2013).
[6] A. G. P. Troeman, H. Derking, B. Borger, J. Pleikies, D. Veldhuis, and H. Hilgenkamp, Nano Lett. **7**, 2152 (2007).
[7] L. Hao, J. C. Macfarlane, J. C. Gallop, D. Cox, J. Beyer, D. Drung, and T. Schurig, Appl. Phys. Lett. **92**, 192507 (2008).
[8] Nicholas C. Koshnick, Martin E. Huber, Julie A. Bert, Clifford W. Hicks, Jeff Large, Hal Edwards, and Kathryn A. Moler, Appl. Phys. Lett. **93**, 243101 (2008).
[9] M. Tinkham, Introduction to Superconductivity 2nd ed. (Mc Graw-Hill, New York, 1996).
[10] D. Hazra, Hysteresis in superconducting weak links and micron size superconducting interference devices, PhD thesis, IIT Kanpur (2011).
[11] Y. Song, J. Appl. Phys. **47**, 2651 (1976); S. Michotte, S.

Mátéfi-Tempfli, L. Piraux, D. Y. Vodolazov and F. M. Peeters, Phys. Rev. B **69**, 094512 (2004).
[12] H. Courtois, M. Meschke, J. T. Peltonen, and J. P. Pekola, Phys. Rev. Lett. **101**, 067002 (2008).
[13] R. Arpaia, M. Arzeo, S. Nawaz, S. Charpentier, F. Lombardi, and T. Bauch, Appl. Phys. Lett. **104**, 072603 (2014).
[14] W. J. Skocpol, M. R. Beasley, and M. Tinkham, J. Appl. Phys. **45**, 4054 (1974).
[15] M. Tinkham, J. U. Free, C. N. Lau, and N. Markovic, Phys. Rev. B **68**, 134515 (2003).
[16] D. Hazra, L. M. A. Pascal, H. Courtois, and A. K. Gupta, Phys. Rev. B **82**, 184530 (2010).
[17] K. S. Ilin, M. Lindgren, M. Currie, A. D. Semenov, G. N. Goltsman, R. Sobolewski, S. I. Cherednichenko and E. M. Gershenzon, Appl. Phys. Lett. **76** , 2752 (2000).
[18] N. Shah, D. Pekker, and P. M. Goldbart, Phys. Rev. Lett **101**, 207001 (2008).
[19] L. Angers, F. Chiodi, G. Montambaux, M. Ferrier, S. Guéron, H. Bouchiat, and J. C. Cuevas, Phys. Rev. B **77**, 165408 (2008).
[20] S. K. H. Lam and D. L. Tilbrook, Appl. Phys. Lett. **82**, 1078 (2003).
[21] R. F. Broom and E. H. Rhoderick, Brit. J. Appl. Phys. J. Phys. **11**, 292 (1960).
[22] See the supplemental Information.
[23] We get the depairing current [9], $I_d = 2A(2/3)^{3/2}[Hc(0)/\lambda]$ as 1.8 mA at 0 K by using penetration depth (λ) as 200nm, thermodynamic critical field $[\mu_0 H_c(0)]$ as 0.2 T and cross-section area (A) for each WL as 31×70 nm^2.
[24] T. A. Fulton and L. N. Dunkelberger, Phys. Rev. B **9**, 4760 (1974).
[25] P. Dubos, H. Courtois, B. Pannetier, F. K. Wilhelm, A. D. Zaikin, and G. Schön, Phys. Rev. B **63**, 064502 (2001);

Supplementary Information

Fabrication Details

We fabricated μ-SQUIDs from Nb films using electron beam lithography. After cleaning the Si substrate with an oxygen plasma, we deposited a 31 nm thick Nb film using e-beam evaporation in a UHV system. We then patterned the structures with electron beam lithography followed by deposition of a 20 nm thick Al film. A lift-off then transferred the pattern to the Al film, which acts as a mask during the reactive ion etching of Nb using SF_6 plasma. Finally, the Al film was removed chemically.

SQUID oscillations with magnetic flux

Figure 5 below shows the oscillations in I_c for μS1 at 4.25 K (below T_h) and in voltage at 7.4 K (above T_h) with external magnetic flux. The voltage oscillations are acquired at a bias current of 0.17 mA, which is close to the critical current at this 7.4 K. The SQUID oscillations

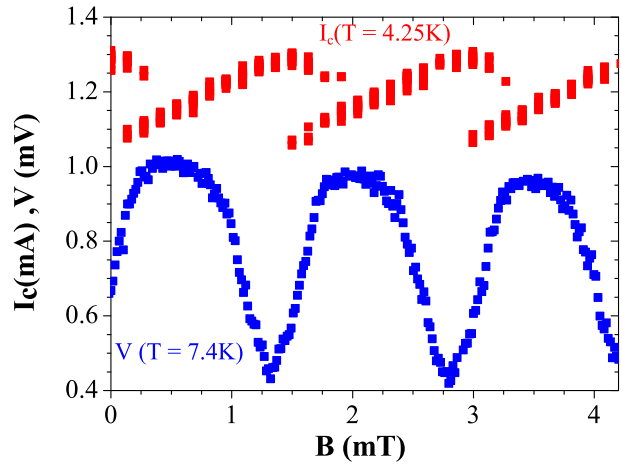

FIG. 5: I_c oscillations in hysteretic regime for μS1 at 4.25K (Red curve) and the voltage oscillations (at 0.17mA current) in non-hysteretic regime at 7.4K (Blue curve).

with magnetic field are seen only in I_c and not in I_{r1} and I_{r2}. The temperature dependent I_c values have been extracted from these I_c-Vs-B plots at all temperatures by selecting maximum I_c at each temperature. In the non-hysteretic regime I_c was found from the maximum slope of the IVC. This is found to coincides with the current at which the voltage modulation in V-Vs-B peaks. In both cases, the magnetic field periodicity is found to be 1.5 mT, which defines an effective SQUID loop area as $A_{eff} = \frac{\phi_0}{\Delta B} = 1.3\mu m^2$, which is larger than the actual patterned (internal) area of 1 μm^2.

Heat sharing during resistive fluctuation

In order to elaborate on the sharing of the extra resistive heat, when the differential element becomes normal, by the three interfaces, we also consider two neighboring differential elements of the same length dx as shown in Fig. 2(b) of the main paper. The one on the left (i.e. from $x = -dx$ to $x = 0$) is at temperature $T_c + dT_1$ and the one on the right (i.e. from $x = dx$ to $x = 2dx$) is at temperature $T_c - dT_2$. The left one gives heat $\dot{Q}_0 = \kappa wt\frac{dT_1}{dx}$ to the middle one, which gives heat $\dot{Q}_1 = \kappa wt\frac{dT_2}{dx}$ to the element on right and thus we get,

$$\kappa wt\frac{dT_1}{dx} = \alpha(T_c - T_b)wdx + \kappa wt\frac{dT_2}{dx} \qquad (2)$$

When the middle element becomes resistive due to fluctuations its temperature increases to $T_c + dT$. In this case the above equation gets modified to

$$\begin{aligned}\kappa wt\frac{dT_1 - dT}{dx} &= \alpha(T_c + dT - T_b)wdx \\ &+ \kappa wt\frac{dT_2 + dT}{dx} - I^2\frac{\rho_n}{wt}dx \qquad (3)\end{aligned}$$

Subtracting eq. 2 from eq. 3 we get $2\kappa wt\frac{dT}{dx} = I^2\frac{\rho_n dx}{wt} - \alpha dTwdx$. Neglecting the higher order second term on the right, we get $\kappa wt\frac{dT}{dx} = I^2\frac{\rho_n dx}{2wt}$. Thus the heat current incident from the left interface, i.e. $\dot{Q'}_0 = \kappa wt\frac{dT_1 - dT}{dx} = \dot{Q}_0 - I^2\frac{\rho_n dx}{2wt}$ and the heat current incident at the right interface, i.e. $\dot{Q'}_1 = \kappa wt\frac{dT_2 + dT}{dx} = \dot{Q}_1 + I^2\frac{\rho_n dx}{2wt}$. Thus the extra heat generated is equally shared across the two interfaces.